

Identification of chemicals that mimic transcriptional changes associated with autism, brain aging and neurodegeneration

Brandon L. Pearson^{1,2#}, Jeremy M. Simon^{1,2#}, Eric S. McCoy¹, Gabriela Salazar¹, Giulia Fragola¹, Mark J. Zylka^{1,2,*}

¹, Department of Cell Biology and Physiology

UNC Neuroscience Center

University of North Carolina at Chapel Hill

111 Mason Farm Rd. Chapel Hill, NC 27599-7545

², Carolina Institute for Developmental Disabilities

University of North Carolina Chapel Hill

Chapel Hill, NC 27599-7255

[#], These authors contributed equally to this work

^{*}, Correspondence to: zylka@med.unc.edu

Abstract

Environmental factors, including pesticides, have been linked to autism and neurodegeneration risk using retrospective epidemiological studies. Here, we sought to prospectively identify chemicals that share transcriptomic signatures with neurological disorders by exposing mouse cortical neuron-enriched cultures to hundreds of chemicals commonly found in the environment and on food. We find that rotenone, a pesticide associated with Parkinson's disease risk, and certain fungicides, including pyraclostrobin, trifloxystrobin, famoxadone, and fenamidone, produce transcriptional changes in vitro that are similar to those seen in brain samples from humans with autism, advanced age and neurodegeneration (Alzheimer's disease, Huntington's disease). These chemicals stimulate free radical production and disrupt microtubules in neurons, effects that can be reduced by pretreating with a microtubule stabilizer, an antioxidant, or with sulforaphane. Our study provides an approach to prospectively identify environmental chemicals that transcriptionally mimic autism and other brain disorders.

Introduction

Powerful new sequencing technologies have been used to systematically identify hundreds of candidate gene mutations associated with autism spectrum disorder (ASD) risk^{1,2}. Heritability studies suggest that environmental factors also contribute to autism risk³. Indeed, gestational exposure to pesticides, including maternal proximity to pesticide applications and runoff, is reproducibly associated with increased ASD risk in epidemiological studies⁴⁻⁶. However, epidemiological studies are retrospective and cannot ascertain prospectively, precisely or systematically which chemicals, of the >80,000 chemicals registered for use in the environment, have the greatest potential to harm the developing or adult brain⁷. Existing *in vivo* neurodevelopmental and neurotoxicological assays with animal models are labor intensive and costly, thus hindering throughput, whereas higher throughput toxicological assays frequently utilize non-neuronal cells or focus on neuron death as an endpoint^{8,9}. As a result, these tests fail to interrogate molecular and physiological processes that are unique to neurons or that differentiate normal from diseased human brains.

There is growing recognition that brain transcriptional changes are associated with ASD^{10,11}. This ASD transcriptional signature is defined by reduced expression of genes involved in synaptic transmission and elevated expression of genes involved in immune and microglial function^{10,11}. Here, we hypothesized that this transcriptional signature might guide the prospective identification of candidate chemical risks for ASD. To test this hypothesis, we exposed mouse cortical neuron-enriched cultures to hundreds of environmental-use chemicals and then monitored global transcriptional changes. We identify six chemical groups, one of which mimics the transcriptional changes seen in ASD, but surprisingly also shares transcriptional similarity to the aged brain and certain neurodegenerative conditions. Our findings suggest these neurological conditions share a molecular pathology, as hypothesized by others¹², despite different ages of onset and distinct behavioral symptoms. Moreover, our study shows that a transcriptional approach can be used to systematically scan a diverse chemical space and identify potential environmental threats to the human brain.

Results

Mouse cortical cultures transcriptionally model human brain

To determine if mouse cortical cultures model cellular and molecular aspects of the human brain, we performed immunocytochemistry with cellular markers and compared the gene expression profile of our cultures to brain cell-type-specific expression data sets and human brain gene expression data sets, including the Allen BrainSpan atlas (www.brainspan.org) and GTEx^{13,14}. Our cultures contained many of the principle cell types of the brain based on immunocytochemistry with markers for neurons, astrocytes and microglia (approximately 25% of cultures were non-neuronal cells; Fig. 1a–b). Additionally, the expression of markers for each brain cell type (Ref. 13) in our cultures was highly correlated with that of whole embryonic (E14.5) brain (Pearson $r = 0.8$), further suggesting that our culture system represented all major cell classes in biologically realistic proportions (Fig. 1c; Supplementary Fig. 1a–b). Globally, gene expression in our cortical cultures correlated more strongly with each human brain region (except spinal cord) than to any other tissues of the human body (Supplementary Fig. 2a). The strongest correlations were to frontal cortex and anterior cingulate cortex, regions implicated in ASD³. Moreover, cultures were most strongly correlated with frontal cortex from mid-late gestation human brain (Supplementary Fig. 2b), the developmental time window implicated in ASD pathogenesis¹⁵. In contrast, terminally differentiated neurons derived from human embryonic stem cells (Ref. 16) did not strongly correlate with any brain region, and instead were most similar to tissues associated with the female reproductive system (Supplementary Fig. 2c). Taken together, our cortical cultures show strong transcriptional similarities to the human brain.

Transcriptional screen with environmental chemicals

We next measured cytotoxicity of the 294 chemicals in the U.S. Environmental Protection Agency (EPA) ToxCastTM Phase I library, which includes common food-use pesticides and other environmental chemicals such as plasticizers⁸, to identify a non-toxic concentration for RNA-seq. We treated cultures

in quadruplicate for 24 h at 10 μ M, as this is a common concentration used in screening studies¹⁷, then used fluorescent markers to quantify the proportion of live and dead cells (Supplementary Fig. 3). Most (87%) of the chemicals were not cytotoxic at 10 μ M whereas concentrations of the remaining chemicals had to be reduced to between 10 nM and 100 nM (Supplementary Data 1). Fresh cultures were then treated (24 h) with each chemical at the non-toxic concentration or with vehicle (equivalent DMSO concentration $\leq 0.5\%$) as the negative control. We also tested three topoisomerase 1 (TOP1) inhibitors, as they reproducibly downregulate long (>100 kb) genes¹⁸.

To identify chemicals that caused concordant gene expression changes, we performed hierarchical clustering of 5,121 genes variably expressed across all chemicals, and six chemical groups emerged (hereafter referred to as Clusters 1–6) (Fig. 2; see Methods and Supplementary Fig. 4 for batch correction details). Individual chemicals were assigned to a cluster using a pairwise correlation threshold and were validated to be statistically and biologically significant (Supplementary Fig. 5; see Methods for further details on inclusion/exclusion criteria). To evaluate whether existing *in vitro* ToxCastTM assay data could identify similar chemical relationships, we performed clustering analysis across 199 cell-free and cellular (non-neuronal) assays. The resulting chemical groupings did not resemble those we detected by gene expression profiling (Supplementary Fig. 6). Thus, transcriptional profiling with neuronal cells identifies relationships between chemicals that existing toxicological assays failed to detect.

To determine what these functional relationships were, we examined specific genes with altered expression in each cluster (Fig. 2). Cluster 1 chemicals upregulated immediate early genes (IEGs) while reducing expression of several potassium channel genes. These expression changes were suggestive of neuronal hyperexcitability. Supporting this possibility, Cluster 1 included two pyrethroids (cyfluthrin, fenpropathrin) that stimulate sustained calcium influx in cortical neurons¹⁹. Cluster 2 chemicals upregulated numerous immune and cytoskeletal transcripts but reduced expression

of ion channel and synaptic genes. Cluster 3 chemicals upregulated IEGs but reduced the expression of immune and cytoskeletal genes. Cluster 4 chemicals resembled Cluster 3, but without inducing IEGs. Cluster 5 contained all three TOP1 inhibitors, which markedly downregulated long genes and downregulated IEGs, consistent with one of these inhibitors (topotecan) reducing spontaneous synaptic activity in cortical neuron cultures²⁰. Deletion of a related topoisomerase (TOP2B) reduced IEG expression²¹. Cluster 6 chemicals reduced expression of several neurotransmitter receptor subunits, including NMDA receptor subunits (*Grin2a*, *Grin2b*), cholinergic receptors (*Chrm2*, *Chrna7*), and ion channels.

Cluster 2 transcriptionally mimics neurological conditions

We next identified molecular pathways that were differentially associated with the six chemical clusters using Gene Set Analysis (GSA). Included in this analysis were 64 gene sets for human brain disorders and nervous system pathways that we generated from publications (Supplementary Data 2) alongside 4,722 curated pathways. Over 600 gene sets distinguished the six clusters (Supplementary Fig. 7, Supplementary Data 3), including many of the human brain disorder gene sets (Fig. 3).

However, only Cluster 2 chemicals mimicked the transcriptional changes of two post-mortem ASD brain expression datasets in a bidirectional manner. This included downregulation of M12 and Mod1 (largely composed of synaptic genes that are downregulated in ASD brains), and upregulation of M16 and Mod5 (largely composed of microglial/immune genes that are upregulated in ASD brains)^{10,11}. Additionally, Cluster 2 showed concordance with aging human brain and two neurodegenerative disorders (Alzheimer's disease and Huntington's disease), suggesting shared aspects of molecular pathology despite different symptoms (see Discussion).

Fenamidone, pyraclostrobin, and two other chemicals in Cluster 2 (famoxadone, trifloxystrobin) are members of a recently developed class of fungicides that inhibit mitochondrial complex III by targeting the quinone outside (Qo) site of cytochrome *bc₁* (Ref. 22). Since fenamidone and

pyraclostrobin are structurally distinct (Fig. 4a-b), we performed RNA-seq with multiple replicates of both chemicals to further validate that expression of a common set of genes was altered. Each fungicide altered expression of a largely overlapping set of genes (Fig. 4c-d, Supplementary Data 4). Upregulated transcripts included *Nrf2* target antioxidant response genes and *Rest*, which we validated using quantitative real-time polymerase chain reaction (qRT-PCR) (Fig. 4e-f). *Rest* elevation is associated with human brain aging and neurodegeneration²³. Other compounds in Cluster 2 include fenpyroximate, pyridaben, and rotenone; chemicals that target mitochondrial complex I²⁴. Exposure to rotenone is known to increase risk for Parkinson's disease^{24,25}. All Cluster 2 chemicals reduced RNA-seq reads arising from the mitochondrial genome (Fig. 2), suggesting compromised mitochondrial function as a common mechanism²⁶. Note that none of the mitochondrially-encoded transcripts were among the 5,121 variably expressed genes assayed by hierarchical clustering, so these transcripts did not influence cluster assignment. However, the influence of chemical treatment on mitochondrial density or viability was not assessed and could have indirectly modulated transcriptional profiles.

Cluster 2 induces superoxide and microtubule instability

Mitochondrial complexes I and III are the main sites of superoxide (O_2^-) production within the electron transport chain, so we next tested whether Cluster 2 chemicals induced O_2^- . Fenamidone produced a concentration-dependent increase in O_2^- , as measured with a fluorescent mitochondrial superoxide indicator dye, and swelling of neuronal soma (Fig. 5a-d). Pre-treatment with the free-radical scavenger vitamin E (α -tocopherol) blocked fenamidone-induced production of O_2^- (Fig. 5e; using the concentration of fenamidone that was used for sequencing) and blocked soma swelling (Fig. 5f). Sulforaphane is a potent inducer of *Nrf2* target antioxidant gene expression, it reduces inflammation, and it substantially reduces autism symptoms in humans^{27,28}. Pretreatment with sulforaphane attenuated the transcriptional changes, O_2^- production, and soma swelling caused by fenamidone (Fig. 6). We also monitored O_2^- production for each chemical in Cluster 2 and for several chemicals outside

of Cluster 2 across a seven-point concentration-response range (Supplementary Fig. 8). All chemicals that induced O_2^- at the sequencing concentration were assigned to Cluster 2 based on gene expression. Fluoxastrobin and azoxystrobin are Qo fungicides that were not assigned to Cluster 2, likely because they did not generate O_2^- at the sequencing concentration (Supplementary Fig. 8). Two additional mitochondrial inhibitors that induce O_2^- production in cells (myxothiazol, complex III inhibitor; kresoxim-methyl, complex III inhibitor and fungicide) altered transcription in a manner consistent with chemicals in Cluster 2 (Supplementary Fig. 9). Collectively, our data support a relationship between O_2^- production and the Cluster 2 transcriptional signature.

Numerous genes associated with cytoskeletal function have been implicated in autism²⁹. Moreover, disruption of microtubules is associated with problems in brain development and with neurodegeneration^{30,31}. Given that cytoskeletal genes were altered by Cluster 2 chemicals and that rotenone (also in Cluster 2) destabilizes microtubules^{31,32}, we hypothesized that microtubule depolymerization triggered the aberrant swelling morphology of neurons. Consistent with this possibility, stabilization of microtubules with paclitaxel attenuated fenamidone-induced O_2^- production and fenamidone-induced soma swelling (Fig. 5g–h). However, fenamidone did not impair tubulin polymerization in a cell-free biochemical assay, ruling out a direct effect of fenamidone on tubulin oligomerization (Supplementary Fig. 10a). Lastly, superoxide production and soma swelling could be phenocopied by depolymerizing microtubules with vincristine (Supplementary Fig. 10b–e).

Assessment of potential confounds

Cluster 2 compounds upregulated numerous microglial- (e.g. *Cx3cr1* and *Trem2*) and astrocyte- (e.g. *Gfap* and *Aqp4*) enriched genes³³. This increase in markers of proliferating brain cell types was unlikely to be due to cell division, as our cultures were treated with an antimitotic on DIV 3. Moreover, fenamidone (under the same conditions used for sequencing) caused no significant change in cellular composition, based on immunocytochemical quantification of neurons, astrocytes, and

microglia with markers (NeuN, Gfap, Iba1, respectively) (Supplementary Fig. 11a). However, any contribution by additional non-neuronal cell types such as oligodendrocytes has not been accounted for. Neither culture batch nor sequencing batch effects contributed to cluster identity (Supplementary Fig. 4). We also assessed RNA quality using the RNA integrity number (RIN) as a proxy. There were subtle differences in quality among the six clusters, and RINs were significantly lower for Clusters 2 and 6 (Supplementary Fig. 11b). However, the average RINs were ≥ 9.25 for each of the six clusters, indicating that these samples were of sufficiently high quality. Collectively, we found no evidence that technical artifacts or poor RNA quality contributed to cluster identity. However, we cannot exclude the possibility that some of the chemicals alter cellular composition at higher concentrations or after longer exposure times.

Increasing agricultural use of several Cluster 2 chemicals

Epidemiological and human exposure data for most chemicals in Cluster 2 are lacking. We thus sought to evaluate exposure potential by analyzing chemical usage and food commodity residue data collected by the United States Geological Survey (USGS), the United States Department of Agriculture (USDA) and the Food and Drug Administration (FDA). All of the mitochondrial complex III inhibitors in Cluster 2 showed positive environmental usage trends since their EPA registration in 2000 or later (Fig. 7). Usage of complex I inhibitors (rotenone, pyridaben) is low and unchanging, with the notable exception of fenpyroximate, the most potent superoxide producer we identified ($EC_{50}=0.007 \mu\text{M}$; Supplementary Fig. 8b). Many Cluster 2 residues were found on conventionally raised food commodities, particularly leafy green vegetables, and were detected at relatively high levels, up to 20 ppm in the case of pyraclostrobin. These data suggest significant human exposure potential to many of the chemicals in Cluster 2.

Discussion

By comparing gene expression profiles of cortical cell cultures with expression data from human brain disorders, we identified a group of eight chemicals (Cluster 2) that transcriptionally mimicked ASD, brain aging, and neurodegeneration. These chemicals, most of which inhibit mitochondrial complex I or III, stimulated free radical production and disrupted microtubules. We found that pretreating with a microtubule stabilizer, an antioxidant, or with sulforaphane could reduce these effects. Whether this transcriptional and cellular response is related to the marked clinical efficacy of sulforaphane at treating ASD symptoms (Ref. 27) remains to be determined.

Numerous studies investigated a link between the inhibition of mitochondrial complex I, neurotoxicity, and neurodegeneration in animal models^{24,34,35}. Rotenone (in Cluster 2) has been shown to increase Parkinson's disease risk in humans²⁵. Cluster 2 also included a relatively new class of fungicides (quinone outside, Qo) that inhibit mitochondrial complex III. No evidence of neurotoxicity was noted for two of these fungicides, pyraclostrobin and fenamidone, in a set of assays used by regulatory agencies^{36,37}. However, a single oral dose of trifloxystrobin (also in Cluster 2) reduced motor activity for several hours in female rats and for three days in males³⁸, suggesting a strong interaction with sex. Picoxystrobin (not in ToxCast Phase I library), marketed as the most rapidly absorbed and most systemic (in plants) of all Qo fungicides, caused acute neurotoxicity (reduced motor activity) at the lowest dose tested in rats³⁹. Further, mitochondrial complex III deficient mice showed severe superoxide-dependent damage to cortical brain regions and profound motor deficits that were apparent at night, during their active phase⁴⁰. Note that standard acute and chronic neurotoxicity assays are performed during the day, when rodents are less active, possibly reducing power to detect motor deficits. Mitochondrial complex III inhibitors can additionally block neuronal differentiation by maintaining embryonic stem cell pluripotency⁴¹, suggesting a potential for neurodevelopmental effects.

Usage data indicate that Qo fungicides are increasingly prevalent on food that is consumed by humans of all ages. At least one Cluster 2 chemical (pyraclostrobin) is present in the environment at

levels that affect non-mammalian organisms^{42,43} and was detected at high levels on foraging honeybees, further corroborating high levels in the environment⁴². To address whether these levels are a risk to human health, recent *in vitro* reverse dosimetry extrapolations from the EPA found that food levels of pyraclostrobin exceed the human oral equivalent dose necessary to affect mitochondrial processes⁴⁴. However, Qo fungicide residues have not been detected on organically produced foods (EPA and USDA data), suggesting a way to minimize exposure.

Our finding that Cluster 2 chemicals mimic the transcriptional changes of autism, as well as the aging brain and neurodegeneration was surprising, particularly given the different ages of onset and disease symptoms. Oxidative stress and cytoskeletal integrity are implicated in all of these conditions^{12,45-49}, suggesting that overlapping pathological processes might drive the transcriptional similarities we observed. In support of shared biology, we found that ASD, the aging brain, Alzheimer's disease, and Huntington's disease exhibit altered expression of a common set of genes more so than any of the other neurological gene sets we tested (Supplementary Fig. 12a). Many of the genes that were differentially regulated by pyraclostrobin were also found in the M16 and M12 ASD gene modules (Supplementary Fig. 12b–e). Moreover, when focusing specifically on the genes in these ASD modules, the direction and magnitude by which these genes were dysregulated in ASD patient samples was strongly correlated with that of pyraclostrobin treatment in our cortical cultures (Spearman $r = 0.66$; Supplementary Figure 12f), further suggesting a common mechanism. The fact that these neurological conditions shared a core set of dysregulated genes may contribute to the enrichment observed for Cluster 2 across these diseases. However, we cannot exclude the possibility that molecular pathologies are shared by some but not all of the conditions. Disentangling these relationships is beyond the scope of our current study, but suggests a fruitful area for future research.

Several of the chemicals in Cluster 2 unquestionably kill neurons at higher concentrations (Supplementary Data 1), consistent with other studies^{9,50}. This raises the question of whether Cluster 2 reflects the transcriptional signature of “sick” neurons. We identified several chemicals that killed cells

at multiple concentrations (Supplementary Data 1), yet only those that were associated with O_2^- production, microtubule destabilization and elevated expression of neuroinflammatory genes were assigned to Cluster 2. It thus seems unlikely that Cluster 2 is reflective of chemicals that nonspecifically kill neurons at high doses and sicken neurons at lower doses. In fact, chemicals can kill (and presumably sicken) cells via distinct mechanisms³², with one of these mechanisms being “microtubule destabilization.” Rotenone and vincristine fit within this class³², likely providing additional insights into why paclitaxel (a microtubule stabilizer) attenuated the soma swelling and O_2^- production phenotypes induced by a Cluster 2 chemical (Fig. 5). Our study also shows how systematic transcriptional studies with neurons can uncover new brain- and disease-relevant relationships between chemicals that cannot be identified using existing toxicology assays (Supplementary Fig. 6), including those that rely on cell death as a readout.

We identified additional brain-relevant relationships between chemicals within other clusters. Cluster 1 appears to define a transcriptional signature of neuron hyperexcitability, as evidenced by upregulation of IEGs, a class of genes that mark recently depolarized neurons, and downregulation of potassium channels (which increases neuron excitability when downregulated⁵¹). Cluster 1 contained two pyrethroids that hyperexcite mammalian neurons¹⁹. Intriguingly, two recent epidemiological studies found that pyrethroid exposure doubles the risk for attention deficit hyperactivity disorder (ADHD) in boys^{52,53}. Our transcriptional approach might provide a way to prospectively identify candidate chemical risks for ADHD. Cluster 5 contained all three topoisomerase inhibitors, a class of drugs that downregulated long genes in neurons¹⁸, reduced synaptic activity²⁰, and reduced IEG expression (Fig. 2). Moreover, Cluster 5 is strongly correlated with neurological disease models that feature dysregulated long synaptic gene expression, particularly amyotrophic lateral sclerosis (ALS)⁵⁴ and Rett syndrome^{55,56}.

Though estimates vary, approximately 50% of cells in the adult human central nervous system are neurons⁵⁷. This is in contrast to the embryonic culture system employed here which is comprised of

over 70% neurons. This disparity has the potential to bias physiological signatures and impair the ability to detect some disease relevant processes. Although, our cultures show a very similar representation of brain cell markers relative to embryonic day 14.5 (E14.5) whole mouse brain (Supplementary Fig. 1), suggesting our cortical cultures—dissected at E14.5—contain the major brain cell classes in biologically realistic proportions. Moreover, the model system employed here is amenable to high throughput screens and functional assays¹⁷. Ultimately, candidate chemicals identified with a cortical culture system will require validation in animal models.

In summary, our study shows that chemicals that transcriptionally mimic brain disorders can be identified by profiling gene expression in cortical cultures. This approach may also prove useful in identifying candidate ASD therapeutics, such as sulforaphane, or in identifying drugs that normalize long gene expression, such as topoisomerase inhibitors in Rett syndrome model neurons⁵⁵. While usage and residue levels of Cluster 2 chemicals on conventionally grown foods are increasing, in the absence of causality, it is premature to draw correlations with the increased prevalence of ASD and other brain disorders. Nonetheless, greater scrutiny over whether these new Qo fungicides affect the developing or adult mammalian nervous system (enteric, peripheral, central) or behaviors seems warranted, particularly given their striking mechanistic similarity to rotenone. Ultimately, monitoring steady state levels in the environment, assessing exposure levels and pharmacokinetics, and epidemiological studies will be needed to evaluate whether any of these chemicals pose real neurological threats to humans or increase risk for brain disorders, including ASD.

Methods

Cortical neuron culture

Primary mouse cortical neuron cultures were prepared as previously described from embryonic day 15 (E15) pregnant C57BL/6J (Cat. #000664, Jackson) dams crossed to CAST/EiJ (Cat. #000928, Jackson) males¹⁸. Hybrid cultures are thought to better model genetic variation associated with human populations⁵⁸. Dissociated cells were placed in multiwell plates coated with poly-D-lysine (0.1 mg ml⁻¹) in Neurobasal medium (Life Technologies) containing 5% FBS (Gibco), B27 (17504-044, Invitrogen), Antibiotic-Antimycotic (15240-062, Invitrogen), and GlutaMAX (35050-061, Invitrogen). At days in vitro (DIV) 3 a half medium change was performed with feeding medium identical to the plating medium except that we omitted FBS and included 4.84 µg ml⁻¹ uridine 5'-triphosphate (U6625, Sigma-Aldrich) and 2.46 µg ml⁻¹ 5-fluoro-2'-deoxyuridine (F0503, Sigma-Aldrich) to inhibit mitosis in dividing cells.

Chemicals

The chemical library was donated by the EPA ToxCastTM Program. For verification and replication experiments, the following chemicals were purchased from Sigma-Aldrich: DL- α tocopherol acetate (T3376), DL-sulforophane (S4441), vincristine sulfate salt (V8879), oxyfluorfen (35031), rotenone (45656), fenamidone (33965), pyraclostrobin (33696), trifloxystrobin (46447), myxothiazol (T5580), pyridaben (46047), azoxystrobin (31697), fluoxastrobin (33797), fenpyroximate (31684), and kresoxim-methyl (37899). Famoxadone was purchased from Chem Service, Inc (N-11943). Topotecan hydrochloride was purchased from Tocris (4562). Paclitaxel was purchased from Fisher Scientific (AC32842). All chemical stocks were prepared in DMSO unless otherwise noted. Vehicle samples were prepared with an equivalent DMSO concentration of less than or equal to 0.5% in feeding medium.

Live/dead assay

Cultures were grown on poly-D-lysine coated 96 well plates at a density of 5×10^4 cells per well.

Culture plates were screened for quality by qualitative assessment of density and by confirming low percentage (<10%) of dead cells in control wells as established by the method described below.

Chemicals were applied in quadruplicate by performing a half medium change with a 2x concentration in pre-warmed feeding medium on culture plates meeting these quality criteria, at DIV 7. After 24 h another half medium change was performed with medium containing NucBlue (R37605, Life Technologies) and SYTOX Green (S7020, Life Technologies) dyes according to manufacturer directions. Cells were then rinsed twice with phosphate buffered saline (PBS; 137 mM NaCl, 10 mM Na_2HPO_4 , 1.8 mM KH_2PO_4) and fixed with 4% paraformaldehyde in 0.1 M phosphate buffer for 10 minutes at room temperature. After rinsing an additional two times with PBS the cells were imaged on a Nikon Eclipse Ti epifluorescent microscope at 10X magnification with UV excitation to reveal the NucBlue dye marking all cells, and with FITC filter set to identify dead SYTOX positive cells. Channel-merged color images were imported into ImageJ software (NIH) and converted into RGB-stacks. A manual threshold was performed on the NucBlue channel to yield an image amenable to binary particle analysis. The threshold set for the NucBlue channel was utilized for the SYTOX channel to reduce any potential bias. Particle analysis was performed on each channel for each image to obtain the total number of nuclei and the total number of nuclei from dead cells, respectively. The percentage of dead cells was calculated and averaged across four replicates. All chemicals from the library were initially tested at 10 μM . A concentration causing 10% or greater cell death relative to vehicle was considered toxic. Lower doses were tested by reducing an order of magnitude until a non-toxic dose was identified.

RNA-seq

Cultures were treated with the non-cytotoxic dose of each chemical, by exchanging half of the original medium with chemicals at 2x concentration in pre-warmed feeding medium, on DIV 7 for 24 h in 12-well plates at a density of 5×10^5 cells per well. RNA was isolated with RNeasy plus mini kit (Cat. #74134, Qiagen). RNA yield and quality was determined with a Nanodrop 1000 Spectrophotometer (Thermo Scientific). Samples were further assessed for quality using either an Agilent Bioanalyzer 2100 or TapeStation 2200 to obtain a RNA integrity number (RIN). RIN values exceeding 7 were used for sequencing. RNA samples were used to generate and barcode cDNA libraries using the TruSeq RNA Library Preparation Kit at the UNC High Throughput Sequencing Facility. Pools of 24 multiplexed samples were sequenced per lane on an Illumina HiSeq 2500 using 50 bp paired-end reads.

RNA-seq data processing

RNA-seq reads were filtered using TagDust and aligned to the reference mouse genome (mm9) with TopHat using default parameters^{59,60}. Reads aligning to rRNA genes were removed. Transcript abundance was estimated by computing RPKM using RefSeq gene models aggregated by gene symbol⁶¹. For differential expression analyses, raw counts over RefSeq exons were used, then compared across samples using DESeq⁶².

Hierarchical clustering and cluster membership

RPKM for all RefSeq genes and all samples were filtered such that a given gene had >90% of samples with RPKM >0 and gene length exceeded 500 bp. RPKMs were then \log_{10} transformed, quantile-normalized, median-centered, and effects due to culture or sequencing batch were removed using a mixed model ANOVA. This batch correction step was performed on individual experiments rather than chemical-vehicle ratios to reduce the effects due to variations in culture composition as well as batch-to-batch variations at the level of sequencing. Genes were then median-centered again, and filtered such that their standard deviation exceeded 0.1. Chemical replicates were then combined using

the median. Classes of chemicals were then discovered in two ways. First, we performed hierarchical clustering using average linkage and Pearson correlation distance measures. The boundaries of the discovered classes from clustering were set by computing pairwise Spearman correlations for all samples. A given cluster had to have at least three members with the minimum pairwise Spearman correlation coefficient exceeding 0.2, though cluster members often exceeded a correlation of 0.6 (Supplementary Fig. 5c–d). Seven chemical clusters were discovered, however one was removed due to failing to have a positive silhouette width, a metric of cluster robustness⁶³. These definitions enabled the three positive control topoisomerase inhibitors to form a cohesive group of chemicals with known structural and functional similarity (Cluster 5). None of the culture or sequencing batches contributed to the formation of any one of the final six clusters (Supplementary Fig. 4).

Hierarchical clustering of EPA toxicological assays

AC₅₀ values for all assays and all ToxCast Phase I chemicals were retrieved from the EPA Dashboard. We retained only those assays with data available for 99% of the chemicals and required that a given assay must have at least 5 active chemicals ($AC_{50} \leq 10 \mu M$); 199 assays were retained. We then transformed the data values as described in Sipes et al (Ref. 64) and performed hierarchical clustering to find chemical groups with concordant activity on certain assays.

Pathway analysis

To detect differentially regulated pathways, chemicals within each of the six clusters were separately compared to all other chemicals tested using GSA⁶⁵, supplying a modified gene pathway file that contained all MSigDB C2 annotations as well as gene sets from published gene expression studies in human diseases and mouse models. Nearly all added gene sets were derived directly from the associated publication. Raw data derived from Durrenberger *et al.* were analyzed by applying quantile normalization, and differential expression was detected using SAM using 500 permutations^{66,67}. Some

brain disease gene expression studies had no significantly differentially expressed genes ($q < 0.05$), and hence could not be included in our analysis. For “BLALOCK_ALZHEIMERS_UP”, a gene set included within MSigDB C2, we removed gene symbols that were not included in the RefSeq annotation. The Gupta *et al.* Mod1 pathway was filtered to include genes with a KM1 score of 0.4 or greater¹⁰, to reduce the number of genes in this pathway below 1,500 so it could be analyzed by GSA. A given pathway (size between 10 and 1,500 genes) was considered if it achieved statistical significance ($FDR < 0.1$) for at least one cluster compared to all other chemicals (500 permutations). Expression of a single pathway was then summarized by taking the median expression value across all genes in that pathway for a given chemical. Once the entire data matrix was assembled, pathways were median-centered and hierarchically clustered, while keeping chemical ordering consistent with Fig. 2. Disease-relevant ontologies were then extracted and plotted separately; color was applied based on the pathway enrichment score (blue indicates pathway downregulation, red indicates pathway upregulation), but only for pathways achieving statistical significance ($FDR < 0.1$).

Quantitative real time PCR

Total RNA was extracted and purified using the RNeasy plus mini kit (Qiagen) following the manufacturer's instructions. RNA was quantified using Nanodrop 1000 (Thermo Scientific) and reverse transcribed using iScript Reverse Transcription Supermix (Bio-Rad). Quantitative real-time PCR analysis was performed in technical duplicates using SYBR Green PCR master mix (Applied Biosystems) in a 7500 Real-Time PCR instrument (Applied Biosystems). Ten ng of cDNA were used in each reaction. Fold change of expression of the target RNA in each treatment condition relative to the untreated sample were calculated by raising 2 to the power of $-\Delta\Delta Ct$. $\Delta\Delta Ct$ was calculated by subtracting the ΔCt of the untreated sample to the ΔCt of each treatment condition. The ΔCt of each sample was calculated by subtracting the average Ct of *Gapdh* to the average Ct of the target RNA. The following primers were used at a final concentration of 0.5 μM :

Rest (F 5'- GTGCGAACTCACACAGGAGA -3' R 5'-AAGAGGTTTAGGCCCGTTGT-3'); *Gsta4* (F 5'- CGGCTGGAGTGGAGTTTGAG-3' ; R 5'- CCAAGGGTACTTGGCCGAAA -3'); *Gstm1* (F 5'- CCGTGCAGACATTGTGGAGA -3'; R 5'- CTGCTTCTCAAAGTCAGGGTTG -3'); *Hmox1* (F 5'- AGGCTTTAAGCTGGTGATGGC -3';R 5'- GGGGCATAGACTGGGTTCTG -3') ; *Gapdh* (F 5'- TATGACTCCACTCACGGCAAAT -3'; R 5'- GGGTCTCGCTCCTGGAAGAT-3').

Fluorescence Immunohistochemistry

Mouse cortical neuron cultures were prepared identically as for live/dead and RNA-Seq experiments but at an equivalent density of 2.5×10^5 cells per well in a 24 well plate containing pre-coated glass coverslips. At DIV 7 cells were treated with fenamidone at a concentration of 10 μ M for 24 hours. Coverslip-adherent cells were rinsed, PFA fixed, blocked with 10% donkey serum and probed with the following cell type-specific primary antibodies: Guinea pig anti-NeuN (1:400, ABN90P, Millipore), Goat anti-Gfap (1:1200, ab53554, Abcam) and Rabbit anti-Iba1 (1:400, 019-19741, Wako Pure Chemical Industries). Species-specific AlexaFluor conjugated donkey secondary antibodies (1:200, Life Technologies) were then applied along with Nucblue (Life Technologies) to counterstain all nuclei. Coverslips were inverted into mounting substance (Fluorogel, 17985-10, Electron Microscopy Sciences) and imaged on a Zeiss LSM 710 laser scanning confocal microscope using a 10X objective tiling scan of entire coverslips including three z-planes to account for uneven coverslips. A researcher blind to the experimental conditions of images utilized maximal projected, spliced images to obtain particle counts for the total Nucblue positive nuclei and the NeuN positive neurons using particle analysis in ImageJ. Gfap and Iba1 positive features containing clear Nucblue positive nuclei were manually counted using the count function in Adobe Photoshop.

Mitochondrial superoxide detection and live cell imaging

Cultures were prepared on commercial poly-D-lysine coated glass coverslips (GG-12-pdl, neuVibro) in 24-well plates at a density of 1.5×10^5 cells per well. At DIV 7 cells were treated with chemical or an equivalent DMSO concentration in feeding medium for two hours. Cells were then treated with MitoSOX Red (M36008, Life Technologies) mitochondrial superoxide indicator for 10 minutes at 37°C. Medium containing the dye was aspirated, and the cells rinsed twice with 37°C feeding medium and replaced with 37°C artificial cerebral spinal fluid (ACSF) composed of 150 mM NaCl, 5 mM KCl, 1 mM MgCl₂, 2 mM CaCl₂, 10 mM HEPES, and 10 mM dextrose, pH 7.3. Individual coverslips were transferred to a stage-top perfusion system mounted on an inverted Nikon Ti Eclipse microscope with constant flow of warmed ACSF. 20X images were collected using an Andora Clara CCD camera for DIC and the Texas Red channel to ascertain the mitochondrial superoxide levels with the same exposure across all experiments. ImageJ software (NIH) was used to trace the soma of the cells in brightfield images as regions of interest (ROIs) using the polygon selection tool. ROIs were then superimposed on the fluorescent image and the total cell fluorescence was calculated per ROI to account for the size of the ROI and normalize to background fluorescent levels, as described⁶⁸. Fluorescence intensity was then normalized to average corrected vehicle intensity. At least two non-overlapping fields from each coverslip were collected for each well. ROI tracing was performed by a researcher blind to the experimental condition. For select conditions the proportion of cells showing altered soma morphology was manually calculated per image by the same experimenter performing ROI tracing.

Tubulin polymerization assay

Chemicals were tested in a commercially available cell-free biochemical assay (BK011P, Cytoskeleton, Inc). Briefly, control and experimental solutions were prepared and loaded in duplicate into a warm (37°C) 96-well plate. A solution of purified tubulin and a fluorescent reporter was added to the wells containing the warm substances and placed into a pre-warmed (37°C) Biotek Synergy HT microplate

reader where fluorescence was measured every minute for 60 minutes. Equimolar doses of paclitaxel (included in kit) and vincristine (V8879, Sigma-Aldrich) were included as positive and negative modulators of tubulin polymerization, respectively.

Chemical usage, residue levels and approval data

Usage data were acquired from USGS. Data are reported as total kilograms applied for each chemical across all U.S. counties sampled per year (2000-2012) and a linear trend line was fit beginning in year 2000 or with the registration year (if after 2000). Registration dates for specific pesticide products were obtained from the National Pesticide Information Retrieval System (<http://ppis.ceris.purdue.edu/>). The National Pesticide Information Retrieval System (NPIRS®) is a collection of pesticide-related databases, applications, and websites under the administration of the Center for Environmental and Regulatory Information Systems at Purdue University, West Lafayette, Indiana. NPIRS® obtains product information on a weekly basis from the EPA Pesticide Product Information System (PPIS) website. This PPIS information, including registered use sites and pests listed on the EPA stamped approved label, is disseminated through the NPIRS® member and public websites and is provided for informational purposes only. To ascertain which foodstuffs had the greatest amount of these chemicals, we ranked the five food commodities in descending order of maximum residue level detected using 2008-2012 data from the USDA Pesticide Data Program and the FDA Pesticide Program Residue Monitoring Program.

References

1. De Rubeis, S. *et al.* Synaptic, transcriptional and chromatin genes disrupted in autism. *Nature* **515**, 209-15 (2014).
2. Iossifov, I. *et al.* The contribution of de novo coding mutations to autism spectrum disorder. *Nature* **515**, 216-21 (2014).
3. Chen, J.A., Penagarikano, O., Belgard, T.G., Swarup, V. & Geschwind, D.H. The emerging picture of autism spectrum disorder: genetics and pathology. *Annu Rev Pathol* **10**, 111-44 (2015).
4. Shelton, J.F. *et al.* Neurodevelopmental disorders and prenatal residential proximity to agricultural pesticides: the CHARGE study. *Environ Health Perspect* **122**, 1103-9 (2014).
5. Roberts, E.M. *et al.* Maternal residence near agricultural pesticide applications and autism spectrum disorders among children in the California Central Valley. *Environ Health Perspect* **115**, 1482-9 (2007).
6. Rossignol, D.A., Genuis, S.J. & Frye, R.E. Environmental toxicants and autism spectrum disorders: a systematic review. *Transl Psychiatry* **4**, e360 (2014).
7. Grandjean, P. & Landrigan, P.J. Neurobehavioural effects of developmental toxicity. *Lancet Neurol* **13**, 330-8 (2014).
8. Dix, D.J. *et al.* The ToxCast program for prioritizing toxicity testing of environmental chemicals. *Toxicol Sci* **95**, 5-12 (2007).
9. Regueiro, J., Olguin, N., Simal-Gandara, J. & Sunol, C. Toxicity evaluation of new agricultural fungicides in primary cultured cortical neurons. *Environ Res* **140**, 37-44 (2015).
10. Gupta, S. *et al.* Transcriptome analysis reveals dysregulation of innate immune response genes and neuronal activity-dependent genes in autism. *Nat Commun* **5**, 5748 (2014).
11. Voineagu, I. *et al.* Transcriptomic analysis of autistic brain reveals convergent molecular pathology. *Nature* **474**, 380-4 (2011).
12. Kern, J.K., Geier, D.A., Sykes, L.K. & Geier, M.R. Evidence of neurodegeneration in autism spectrum disorder. *Transl Neurodegener* **2**, 17 (2013).
13. Zeisel, A. *et al.* Brain structure. Cell types in the mouse cortex and hippocampus revealed by single-cell RNA-seq. *Science* **347**, 1138-42 (2015).
14. Consortium, G. Human genomics. The Genotype-Tissue Expression (GTEx) pilot analysis: multitissue gene regulation in humans. *Science* **348**, 648-60 (2015).
15. Willsey, A.J. *et al.* Coexpression networks implicate human midfetal deep cortical projection neurons in the pathogenesis of autism. *Cell* **155**, 997-1007 (2013).
16. van de Leemput, J. *et al.* CORTECON: a temporal transcriptome analysis of in vitro human cerebral cortex development from human embryonic stem cells. *Neuron* **83**, 51-68 (2014).
17. Huang, H.S. *et al.* Topoisomerase inhibitors unsilence the dormant allele of Ube3a in neurons. *Nature* **481**, 185-9 (2012).
18. King, I.F. *et al.* Topoisomerases facilitate transcription of long genes linked to autism. *Nature* **501**, 58-62 (2013).
19. Cao, Z., Shafer, T.J. & Murray, T.F. Mechanisms of pyrethroid insecticide-induced stimulation of calcium influx in neocortical neurons. *J Pharmacol Exp Ther* **336**, 197-205 (2011).
20. Mabb, A.M. *et al.* Topoisomerase 1 inhibition reversibly impairs synaptic function. *Proc Natl Acad Sci U S A* **111**, 17290-5 (2014).
21. Madabhushi, R. *et al.* Activity-Induced DNA Breaks Govern the Expression of Neuronal Early-Response Genes. *Cell* (2015).
22. Bartlett, D.W. *et al.* The strobilurin fungicides. *Pest Management Science* **58**, 649-662 (2002).
23. Lu, T. *et al.* REST and stress resistance in ageing and Alzheimer's disease. *Nature* **507**, 448-54 (2014).

24. Sherer, T.B. *et al.* Mechanism of toxicity of pesticides acting at complex I: relevance to environmental etiologies of Parkinson's disease. *J Neurochem* **100**, 1469-79 (2007).
25. Tanner, C.M. *et al.* Rotenone, paraquat, and Parkinson's disease. *Environ Health Perspect* **119**, 866-72 (2011).
26. Mehrabian, Z., Liu, L.I., Fiskum, G., Rapoport, S.I. & Chandrasekaran, K. Regulation of mitochondrial gene expression by energy demand in neural cells. *J Neurochem* **93**, 850-60 (2005).
27. Singh, K. *et al.* Sulforaphane treatment of autism spectrum disorder (ASD). *Proc Natl Acad Sci U S A* **111**, 15550-5 (2014).
28. Sandberg, M., Patil, J., D'Angelo, B., Weber, S.G. & Mallard, C. NRF2-regulation in brain health and disease: implication of cerebral inflammation. *Neuropharmacology* **79**, 298-306 (2014).
29. Chang, J., Gilman, S.R., Chiang, A.H., Sanders, S.J. & Vitkup, D. Genotype to phenotype relationships in autism spectrum disorders. *Nat Neurosci* **18**, 191-8 (2015).
30. Poirier, K. *et al.* Mutations in TUBG1, DYNC1H1, KIF5C and KIF2A cause malformations of cortical development and microcephaly. *Nat Genet* **45**, 639-47 (2013).
31. Choi, W.S., Palmiter, R.D. & Xia, Z. Loss of mitochondrial complex I activity potentiates dopamine neuron death induced by microtubule dysfunction in a Parkinson's disease model. *J Cell Biol* **192**, 873-82 (2011).
32. Wolpaw, A.J. *et al.* Modulatory profiling identifies mechanisms of small molecule-induced cell death. *Proc Natl Acad Sci U S A* **108**, E771-80 (2011).
33. Zhang, Y. *et al.* An RNA-sequencing transcriptome and splicing database of glia, neurons, and vascular cells of the cerebral cortex. *J Neurosci* **34**, 11929-47 (2014).
34. Greenamyre, J.T., Cannon, J.R., Drolet, R. & Mastroberardino, P.G. Lessons from the rotenone model of Parkinson's disease. *Trends Pharmacol Sci* **31**, 141-2; author reply 142-3 (2010).
35. Mullett, S.J. & Hinkle, D.A. DJ-1 deficiency in astrocytes selectively enhances mitochondrial Complex I inhibitor-induced neurotoxicity. *J Neurochem* **117**, 375-87 (2011).
36. O'Mullane, M. & Tasheva, M. Fenamidone. *JMPR*, 219-270 (2013).
37. Bartholomaeus, A. Pyraclostrobin. *JMPR*, 275-319 (2003).
38. Dannan, G. & Tasheva, M. Trifloxystrobin. *JMPR*, 387-450 (2004).
39. Dewhurst, I. & Solecki, R. Picoxystrobin. *JMPR*, 725-767 (2012).
40. Diaz, F., Garcia, S., Padgett, K.R. & Moraes, C.T. A defect in the mitochondrial complex III, but not complex IV, triggers early ROS-dependent damage in defined brain regions. *Hum Mol Genet* **21**, 5066-77 (2012).
41. Pereira, S.L. *et al.* Inhibition of mitochondrial complex III blocks neuronal differentiation and maintains embryonic stem cell pluripotency. *PLoS One* **8**, e82095 (2013).
42. Pettis, J.S. *et al.* Crop pollination exposes honey bees to pesticides which alters their susceptibility to the gut pathogen *Nosema ceranae*. *PLoS One* **8**, e70182 (2013).
43. Bruhl, C.A., Schmidt, T., Pieper, S. & Alscher, A. Terrestrial pesticide exposure of amphibians: an underestimated cause of global decline? *Sci Rep* **3**, 1135 (2013).
44. Wetmore, B.A. *et al.* Integration of dosimetry, exposure, and high-throughput screening data in chemical toxicity assessment. *Toxicol Sci* **125**, 157-74 (2012).
45. Mota, S.I. *et al.* Oxidative stress involving changes in Nrf2 and ER stress in early stages of Alzheimer's disease. *Biochim Biophys Acta* **1852**, 1428-41 (2015).
46. Valencia, A. *et al.* Elevated NADPH oxidase activity contributes to oxidative stress and cell death in Huntington's disease. *Hum Mol Genet* **22**, 1112-31 (2013).
47. Salminen, L.E. & Paul, R.H. Oxidative stress and genetic markers of suboptimal antioxidant defense in the aging brain: a theoretical review. *Rev Neurosci* **25**, 805-19 (2014).
48. Bamburg, J.R. & Bloom, G.S. Cytoskeletal pathologies of Alzheimer disease. *Cell Motil*

- Cytoskeleton* **66**, 635-49 (2009).
49. DiProspero, N.A. *et al.* Early changes in Huntington's disease patient brains involve alterations in cytoskeletal and synaptic elements. *J Neurocytol* **33**, 517-33 (2004).
 50. Yap, Y.W. *et al.* Gene expression profiling of rotenone-mediated cortical neuronal death: evidence for inhibition of ubiquitin-proteasome system and autophagy-lysosomal pathway, and dysfunction of mitochondrial and calcium signaling. *Neurochem Int* **62**, 653-63 (2013).
 51. Tsantoulas, C. & McMahon, S.B. Opening paths to novel analgesics: the role of potassium channels in chronic pain. *Trends Neurosci* **37**, 146-58 (2014).
 52. Richardson, J.R. *et al.* Developmental pesticide exposure reproduces features of attention deficit hyperactivity disorder. *FASEB J* **29**, 1960-72 (2015).
 53. Wagner-Schuman, M. *et al.* Association of pyrethroid pesticide exposure with attention-deficit/hyperactivity disorder in a nationally representative sample of U.S. children. *Environ Health* **14**, 44 (2015).
 54. Lagier-Tourenne, C. *et al.* Divergent roles of ALS-linked proteins FUS/TLS and TDP-43 intersect in processing long pre-mRNAs. *Nat Neurosci* **15**, 1488-97 (2012).
 55. Gabel, H.W. *et al.* Disruption of DNA-methylation-dependent long gene repression in Rett syndrome. *Nature* **522**, 89-93 (2015).
 56. Sugino, K. *et al.* Cell-type-specific repression by methyl-CpG-binding protein 2 is biased toward long genes. *J Neurosci* **34**, 12877-83 (2014).
 57. Azevedo, F.A. *et al.* Equal numbers of neuronal and nonneuronal cells make the human brain an isometrically scaled-up primate brain. *J Comp Neurol* **513**, 532-41 (2009).
 58. French, J.E. *et al.* Diversity Outbred Mice Identify Population-Based Exposure Thresholds and Genetic Factors that Influence Benzene-Induced Genotoxicity. *Environ Health Perspect* **123**, 237-45 (2015).
 59. Lassmann, T., Hayashizaki, Y. & Daub, C.O. TagDust--a program to eliminate artifacts from next generation sequencing data. *Bioinformatics* **25**, 2839-40 (2009).
 60. Trapnell, C., Pachter, L. & Salzberg, S.L. TopHat: discovering splice junctions with RNA-Seq. *Bioinformatics* **25**, 1105-11 (2009).
 61. Mortazavi, A., Williams, B.A., McCue, K., Schaeffer, L. & Wold, B. Mapping and quantifying mammalian transcriptomes by RNA-Seq. *Nat Methods* **5**, 621-8 (2008).
 62. Anders, S. & Huber, W. Differential expression analysis for sequence count data. *Genome Biol* **11**, R106 (2010).
 63. Rousseeuw, P.J. Silhouettes: a graphical aid to the interpretation and validation of cluster analysis. *J Computational and Applied Mathematics* **20**, 53-65 (1987).
 64. Sipes, N.S. *et al.* Profiling 976 ToxCast chemicals across 331 enzymatic and receptor signaling assays. *Chem Res Toxicol* **26**, 878-95 (2013).
 65. Efron, B. & Tibshirani, R. On testing the significance of sets of genes. *Tech report*, 1-32 (2006).
 66. Durrenberger, P.F. *et al.* Common mechanisms in neurodegeneration and neuroinflammation: a BrainNet Europe gene expression microarray study. *J Neural Transm* (2014).
 67. Tusher, V.G., Tibshirani, R. & Chu, G. Significance analysis of microarrays applied to the ionizing radiation response. *Proc Natl Acad Sci U S A* **98**, 5116-21 (2001).
 68. Burgess, A. *et al.* Loss of human Greatwall results in G2 arrest and multiple mitotic defects due to deregulation of the cyclin B-Cdc2/PP2A balance. *Proc Natl Acad Sci U S A* **107**, 12564-9 (2010).

Acknowledgements

Keith Houck and Richard Judson at the EPA provided the ToxCast library. Margaret Twomey, Alex Carlson and Alice Metz provided technical assistance. Jason Yi provided advice on microtubule assays. This work was supported by NIEHS (DP1ES024088; M.J.Z.), NICHD (5T32HD040127; B.L.P.), NINDS and NICHD (P30NS045892; P30HD031110, J.M.S.).

Author contributions

M.J.Z. and B.L.P. designed the study. B.L.P. performed dosing and RNA preparation experiments. J.M.S. analyzed all RNA-seq data. G.S. and E.S.M. generated cortical cultures. B.L.P. and E.S.M. performed live cell imaging. G.F. performed qRT-PCR experiments. B.L.P., J.M.S., and M.J.Z. wrote the manuscript.

Accession codes

All RNA-seq data have been deposited in GEO under accession number GSE70249.

Competing financial interests

The authors declare no competing financial interests

Figures

Fig. 1. Mouse cortical cultures contain all principle brain cell types. (a–b) Vehicle-treated cortical cultures contain NeuN positive neurons, Gfap positive astrocytes, and Iba1 positive microglia. n= 98,890-145,032 cells/coverglass counted. Values are Mean \pm SEM of 4 biological replicates. Scale bar, 100 μ m. (c) Cortical cultures exhibit expression of marker genes representative of nine cell types found in the brain (y-axis RPKM).

Fig. 2. Gene expression defines six chemical clusters in cortical neuron cultures. Median-centered gene expression values for 297 chemicals and vehicle (v; median of 49 replicates, t; topotecan positive control, median of 32 replicates) were hierarchically clustered across 5,121 variably-expressed genes. Genes >100 kb in length are tick marked (right), and mitochondrial health (bottom) was estimated by comparing the fraction of reads that align to the mitochondrial genome for each chemical-vehicle pair (blue indicates negative \log_2 fold-change with respect to vehicle).

Fig. 3. Cluster 2 chemicals show significant gene set enrichment with autism, aging brain, and neurodegeneration. The enrichment scores of brain disease gene sets that were statistically significant (FDR < 0.1) in each chemical cluster were plotted on a scale from -1 (blue) to +1 (red). Author surname and/or gene set name are indicated in parentheses. The composition of these gene sets is shown in Supplementary Data 2.

Fig. 4. Cluster 2 chemicals alter expression of a common set of genes. (a) Fenamidone and (b) pyraclostrobin (c, d) up- and downregulate a largely overlapping set of genes. RNA-seq was performed in quadruplicate after treating cultured cortical cultures with fenamidone (10 μ M) or pyraclostrobin (0.1 μ M) for 24 h (n=3 biological replicates) and compared to matched vehicle controls

using DESeq to detect differentially expressed genes listed in Supplementary Data 4. Quantitative RT-PCR fold-change (Mean \pm SEM across 3-4 biological replicates) of selected Cluster 2 upregulated genes relative to vehicle after 24 h treatment with (e) 10 μ M fenamidone or (f) the indicated doses of fenamidone.

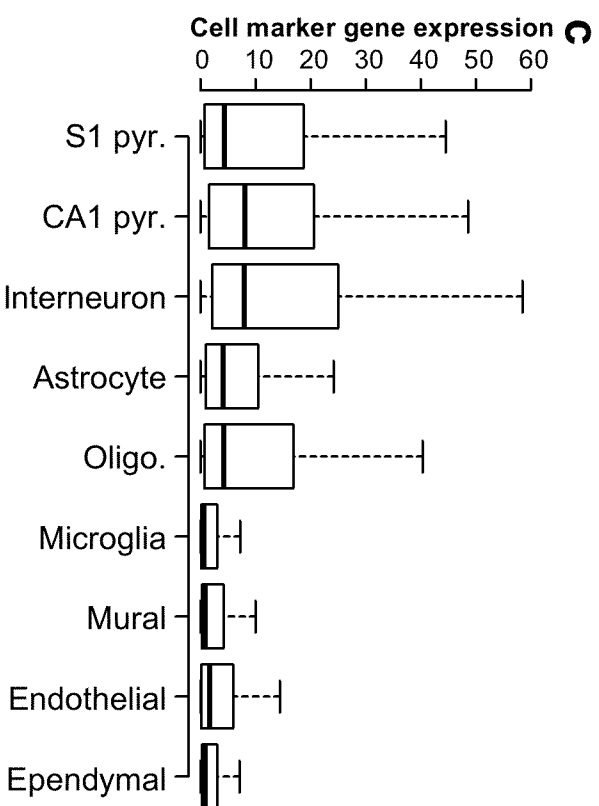
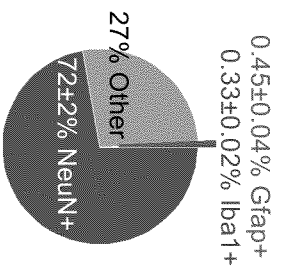
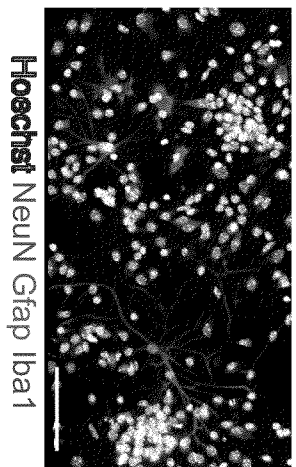
Fig. 5. Fenamidone causes mitochondrial superoxide production and microtubule destabilization.

(a,b) Superoxide (O_2^- , MitoSOX fluorescent indicator) and aberrant cell morphology elicited by 2 h treatment with 10 μ M fenamidone. Scale bars, 10 μ m. (c) O_2^- generation and (d) aberrant morphology is dose-dependent. RNA-seq dose is denoted by red circles. (e) Pre-treatment with vitamin E (10 μ M, 2 h) blocked O_2^- formation and (f) aberrant morphology elicited by fenamidone (10 μ M, 2 h). (g) Microtubule stabilization with paclitaxel pre-treatment (10 μ M, 2 h) attenuated O_2^- formation and (h) aberrant morphology elicited by fenamidone (10 μ M, 2 h). All values mean \pm SEM. n= 33-256 cells/condition across six biological replicates. Bar graphs display Mean \pm SEM. *p<0.05, ***p<0.001, **** p<0.0001.

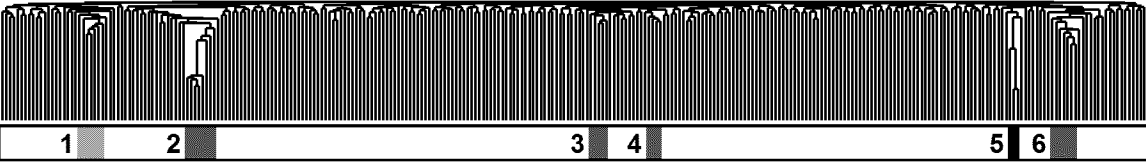
Fig 6. Sulforaphane attenuated fenamidone-induced upregulation of immune/cytoskeletal genes, superoxide production, and cell morphological changes in cortical cultures.

(a) Genome-wide (RNA-seq) transcriptional changes caused by fenamidone (10 μ M, 24 h; n=3 replicates) and fenamidone (10 μ M, 24 h) after pretreating with sulforaphane (10 μ M, 18 h; n=3 replicates). Gene order is identical to Fig. 2. (b) Fenamidone-induced (10 μ M, 2 h) O_2^- production and (c) aberrant cell morphology was attenuated by pretreating (18 h) with two concentrations of sulforaphane (SULF). n=175-327 cells/condition across 6-18 biological replicates. Bar graphs display Mean \pm SEM. **p<0.01, ***p<0.001, **** p<0.0001.

Fig. 7. **Usage trends and environmental fate of Cluster 2 chemicals.** (a-i, left panels) Amount of chemical (alphabetical order) applied in the United States based on USGS data. (a-i, right panels) The five foods with the highest residue levels and the year of detection based on USDA and FDA data spanning 2008-2012. Red arrows indicate the year each chemical was first registered for use with the EPA. Chemicals approved prior to 2000 list the registration year in red font below the x-axis. Spinach tested for high levels of fenamidone in both the 2009 USDA and FDA surveys (c), hence explaining why “Spinach (2009)” is displayed twice.



Chemicals →



Immune **Cytosk.**
Tspo *Acta2*
Cx3Cr1 *Tagln*
Abca1 *Cnn1*
Mki67 *Cnn2*
Tlr13 *Lima1*

Nrf2 targets
Gstm1 *Gsta4*
Hmox1 *Nqo1*

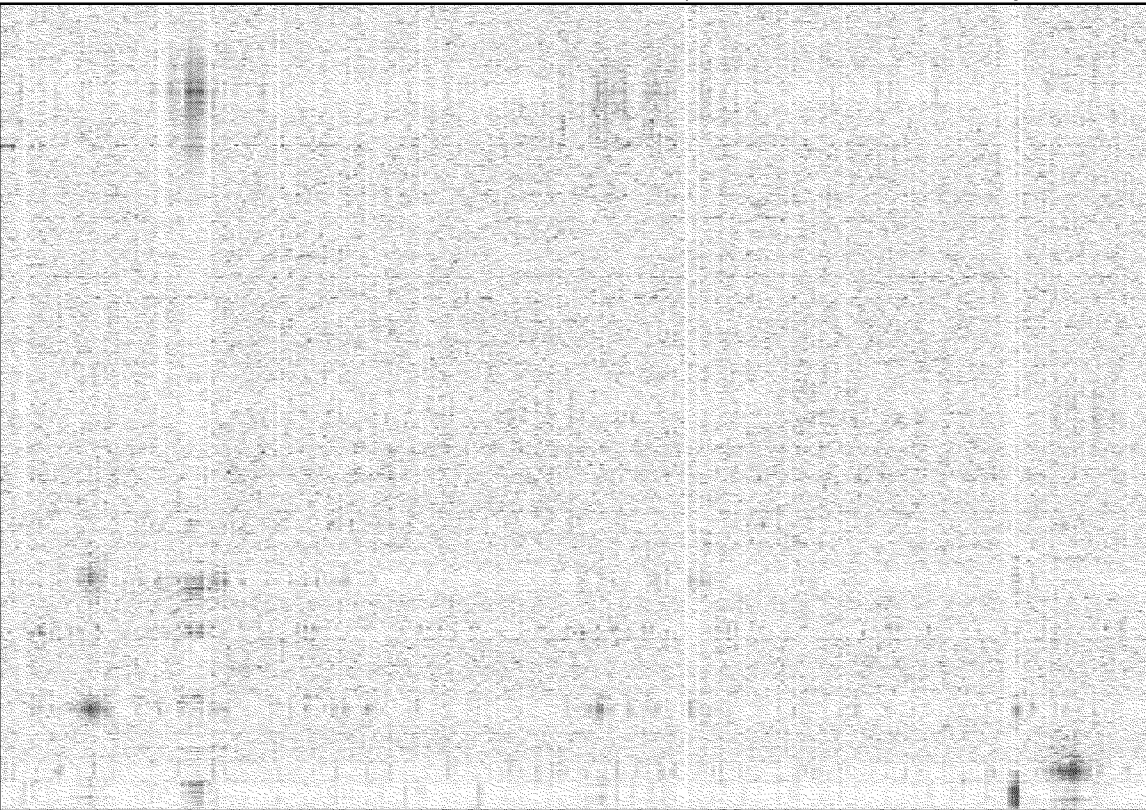
5,121 genes

Ion channels
Kcnn1 *Kcnb2*
Kcnn2 *Kcnh3*

IEG/Hormone
Fos *Bdnf*
Fosb *Crh*
Npas4 *Vgf*

Synaptic **NMDA**
Nlgn1 *Grin2a*
Nrxn3 *Grin2b*
Ctnna2 *Kcna3*

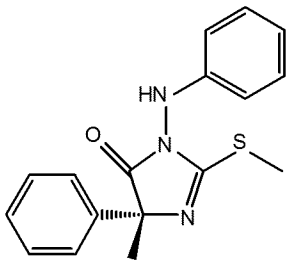
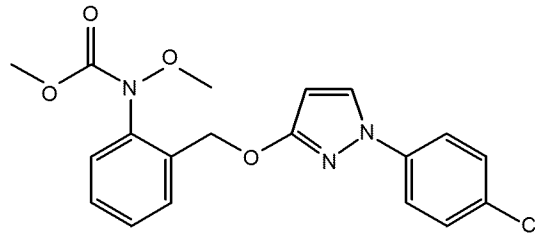
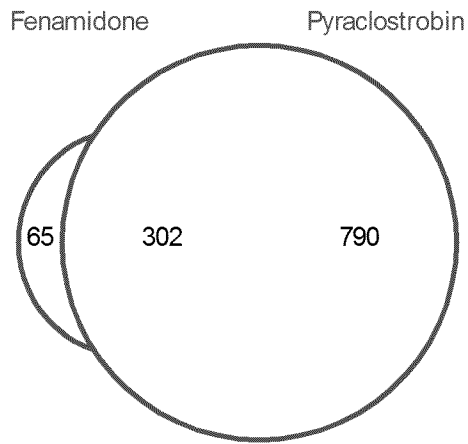
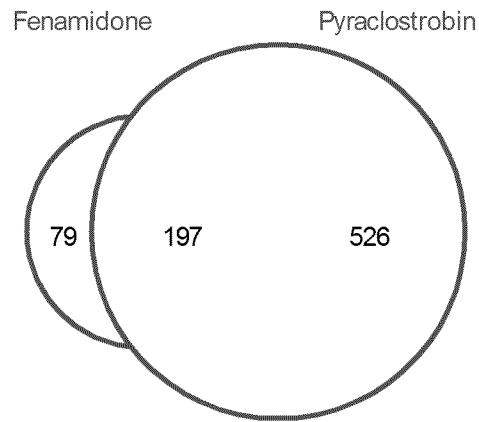
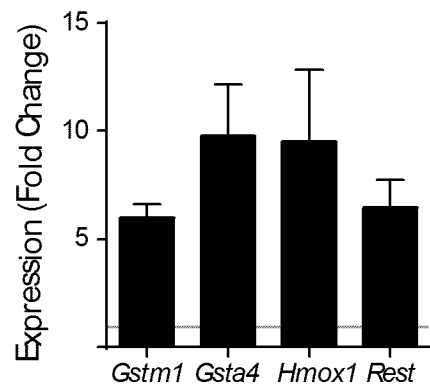
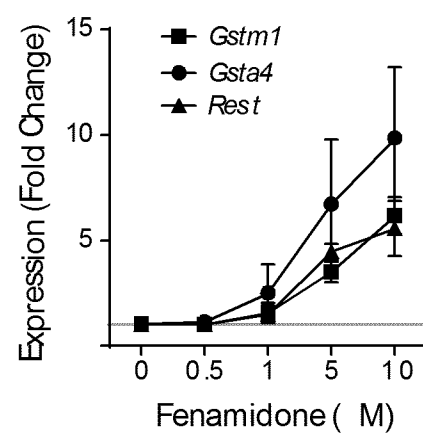
mtDNA

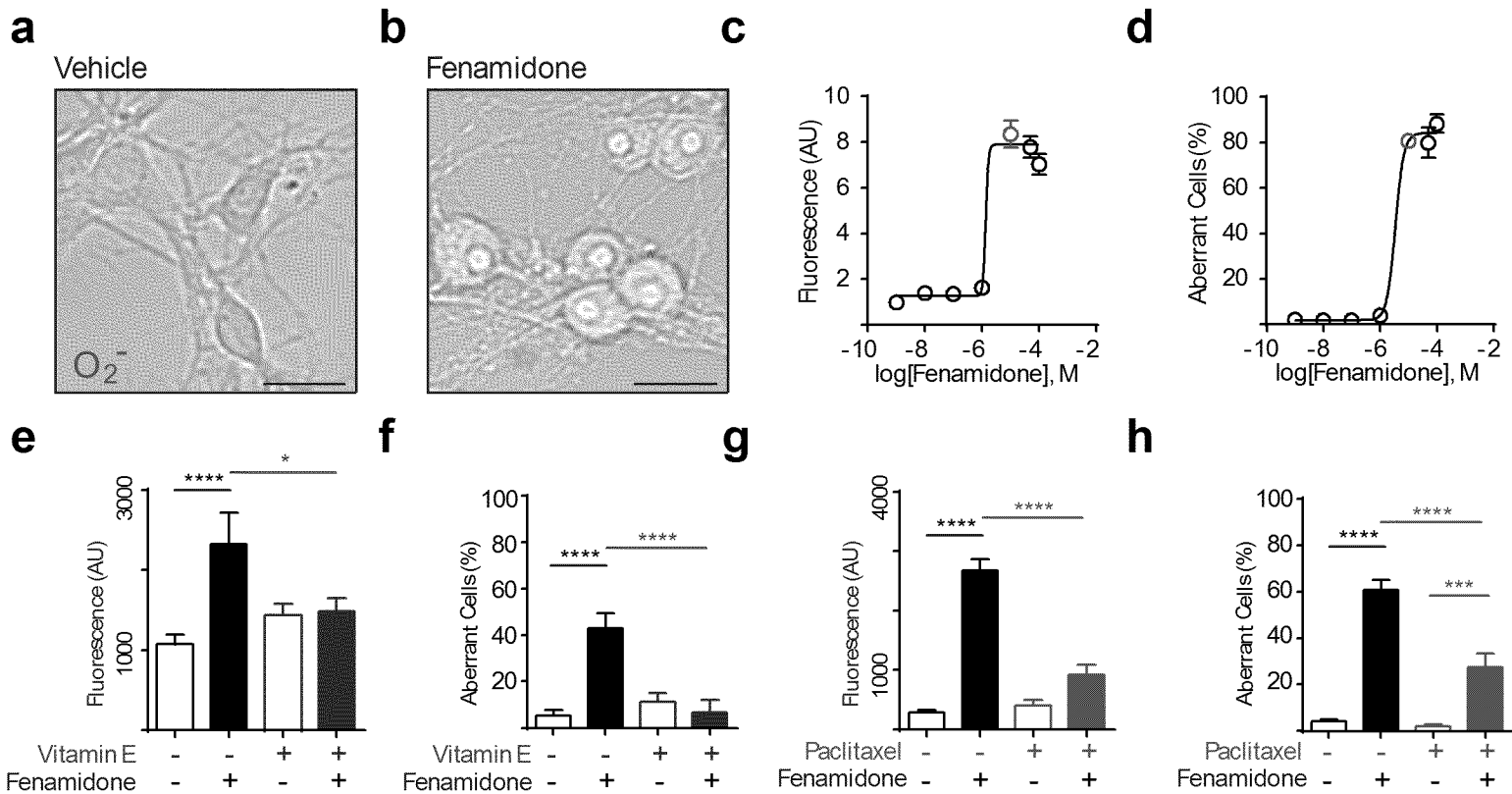


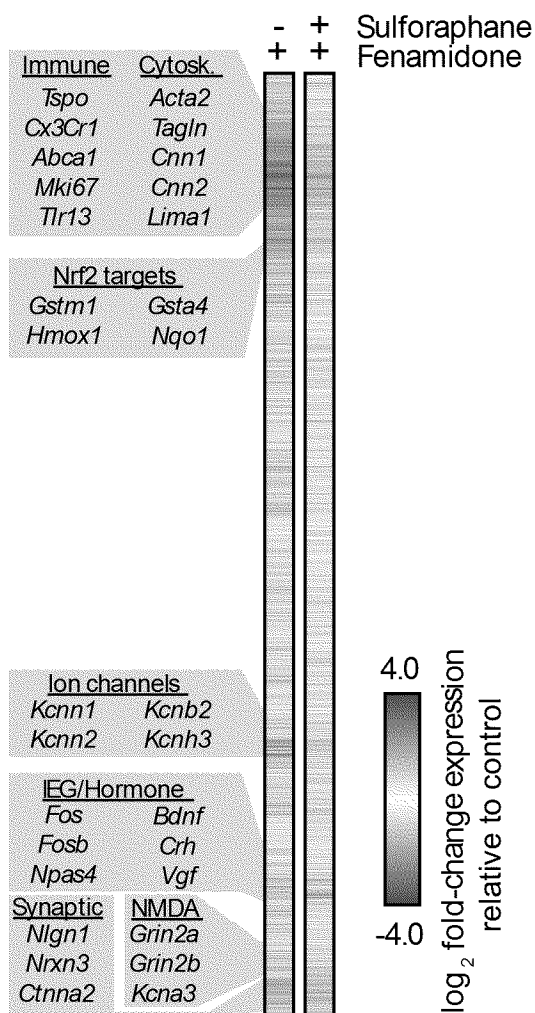
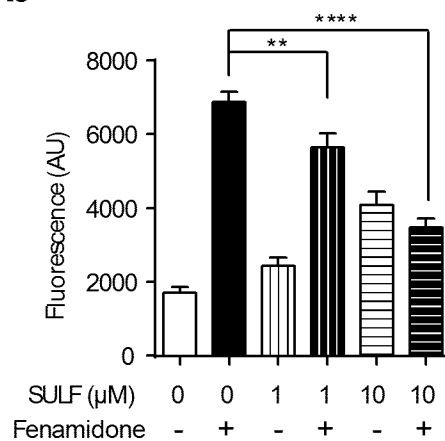
0.5
Median-centered
expression value
-0.5

Pathology	Set Name	1	2	3	4	5	6
Aging Brain	Downregulated (Lu)						
	Upregulated (Lu)						
Amyotrophic Lateral Sclerosis	Downregulated (Durrenberger)						
	Downregulated (Lagier-Tourenne TDP-43 model)						
	Downregulated (Lederer)						
	Upregulated (Lederer)						
Alzheimer's	Downregulated (Blalock)						
	Upregulated (Blalock)						
	Downregulated (Sekar)						
	Upregulated (Sekar)						
	Downregulated (Wu)						
	Upregulated (Wu)						
Autism Spectrum Disorders	Downregulated (Gupta Mod1)						
	Upregulated (Gupta Mod5)						
	Downregulated (Voineagu M12)						
	Upregulated (Voineagu M16)						
Bipolar Disorder	Downregulated (Iwamoto)						
	Upregulated (Iwamoto)						
Huntington's Disease	Downregulated (Durrenberger)						
	Upregulated (Durrenberger)						
	Downregulated (Valor, cerebellum)						
	Upregulated (Valor, cerebellum)						
	Downregulated (Valor, hippocampus)						
	Upregulated (Valor, hippocampus)						
Multiple Sclerosis	Downregulated (Durrenberger)						
Parkinson's Disease	Downregulated (Durrenberger)						
	Upregulated (Durrenberger)						
	Downregulated (Simunovic)						
	Upregulated (Simunovic)						
Rett Syndrome	Downregulated (Chahrour Mecp2 null)						
	Upregulated (Chahrour Mecp2 null)						
	Downregulated (Samaco Mecp2 null)						
	Upregulated (Samaco Mecp2 null)						
Schizophrenia	Downregulated (Barnes, BA22 region)						
	Upregulated (Barnes, BA22 region)						
	Downregulated (Fillman)						
	Upregulated (Fillman)						
	Downregulated (Hwang)						
	Upregulated (Hwang)						
	Downregulated (Maycox)						
	Upregulated (Maycox)						



a**Fenamidone****b****Pyraclostrobin****c**Upregulated**d**Downregulated**e****f**



a**b****c**